Mon. Not. R. Astron. Soc. **310**, 78–86 (1999)

Observations and a model for the infrared continuum of Centaurus A

D. M. Alexander,[1,2★] A. Efstathiou,[3] J. H. Hough,[1] D. K. Aitken,[1] D. Lutz,[4] P. F. Roche[5] and E. Sturm[4]

[1]*Department of Physical Sciences, University of Hertfordshire, Hatfield, Hertfordshire AL10 9AB*
[2]*SISSA, via Beirut 2–4, 34014 Trieste, Italy*
[3]*Astrophysics Group, Imperial College, Blackett Laboratory, Prince Consort Road, London SW7 2BZ*
[4]*Max-Planck-Institut für extraterrestrische Physik, Postfach 1603, 85740 Garching, Germany*
[5]*Department of Astrophysics, University of Oxford, Keble Road, Oxford OX1 3RH*

Accepted 1999 June 28. Received 1999 May 10; in original form 1998 August 5

ABSTRACT

We present ISOSWS, ISOPHOT_S and 8–13 μm observations of Centaurus A which show prominent PAH and silicate features. These and other data are used to construct a model for the infrared continuum. We find that, in a small nuclear aperture (∼ 4 arcsec, ∼ 60 pc), the spectral energy distribution is characteristic of emission from a starburst and dusty AGN torus; in larger apertures, additional components of cirrus and starburst emission are required.

The model components are based on the radiative transfer models of Efstathiou et al. which include multiple scattering and the radiative effects of a dust-embedded source with a distribution of grain species and sizes. The torus component is modelled in terms of a tapered dusty disc centrally illuminated by a quasar-like source. The cirrus and starburst components are, respectively, modelled in terms of diffuse dust illuminated by the interstellar medium and an ensemble of optically thick molecular clouds centrally illuminated by hot stars. These latter components additionally include emission from small graphite particles and PAHs.

Based on our overall model, the torus diameter is estimated to be 3.6 pc and the best inclination angle of the torus is 45°. We present independent observational evidence for this structure. This result has implications for the detectability of tori in low-power AGN and for the use of the *IRAS* 60/25-μm flux ratio as an indicator of the torus inclination.

Key words: radiative transfer – galaxies: active – galaxies: individual: Centaurus A – galaxies: nuclei – galaxies: starburst – infrared: galaxies.

1 INTRODUCTION

Rowan-Robinson & Crawford (1989) attribute the infrared (IR) spectra of galaxies to a mixture of up to three components: (i) general disc emission from dust grains heated by the interstellar radiation field (cirrus); (ii) a Seyfert component peaking in the mid-infrared (MIR); and (iii) a starburst component peaking at about 60 μm.

Essentially all of these sources arise from the thermal reprocessing of ultraviolet (UV) and other high-energy photons from the dust within these objects. The dust grains reradiate the absorbed energy in the IR with the resultant radiation spectrum dependent on the distribution of dust grain temperatures. For the starburst and Seyfert components the clouds of dust are optically thick, even to IR photons, so radiative transfer effects are important.

★ E-mail: davo@sissa.it

The first component suggested by Rowan-Robinson & Crawford is the infrared 'cirrus', generating a distinctive spectrum arising from the reprocessing of light from a combination of illuminating sources within the galaxy – the interstellar radiation field. As is well known, interstellar dust consists of a mixture of large and small grains, as well as large aromatic molecules which respond differently to the interstellar radiation field. The result is a bimodal thermal spectrum: a hot component, including polycyclic aromatic hydrocarbon (PAH) features, produced by the transient heating of small grains by UV photons; and a cooler component produced by the thermal radiation of larger grains. There is ample evidence of cirrus within the Galaxy, such as the observations of diffuse cirrus clouds at high Galactic latitude (Stark 1995). It is not clear whether the cirrus emission is due entirely to diffuse dust in the galaxy or to the 'skins' of molecular clouds.

The second component is generally attributed to the classical optically and geometrically thick torus required by the unified

active galactic nucleus (AGN) scheme to explain the differences between type 1 and type 2 objects (Antonucci 1993). Efstathiou & Rowan-Robinson (1995, hereafter ER95) showed that the torus emission peaks in the MIR. Direct observations of AGN tori are difficult because of their small size, with perhaps the most conclusive observational evidence being that of Young et al. (1996). Their *H*-band polarized flux image of NGC 1068 shows the torus as a band obscuring the scattered flux from the backward-facing cone. The calculated diameter of the torus (~ 200 pc) agrees well with the modelling of Efstathiou, Hough & Young (1995, hereafter EHY).

The third component is thought to arise in regions of intense star formation – the starburst. Roche et al. (1991) have shown that it has a generic form peaking in the far-infrared (FIR). The spectra of starburst galaxies also show the so-called 'unidentified infrared features', now widely attributed to PAH molecules. Models for the starburst (involving ensembles of optically thick giant molecular clouds, centrally illuminated by hot stars) of increasing degree of sophistication have been presented by Rowan-Robinson & Crawford (1989), Rowan-Robinson & Efstathiou (1993), Krügel & Siebenmorgen (1994) and Efstathiou, Rowan-Robinson & Siebenmorgan (1999, hereafter ERS).

In addition to these components, three additional processes can contribute to the IR continuum. Starlight can dominate the near-IR (NIR), but is comparatively negligible at longer wavelengths. Free–free emission can extend from the optical to the radio but is not a large IR contributor, whilst in the FIR and submillimetre the non-thermal power-law continuum from the AGN can make a significant contribution in powerful radio-loud objects.

The objective of this paper is to model the IR to millimetre emission of Centaurus A, using observations from a variety of different aperture sizes, to constrain the emission and dimensions of the putative dusty AGN torus in Centaurus A. The rest of this paper is structured as follows: Section 2 introduces Centaurus A, Section 3 presents the observations and data used, Section 4 describes the model components, Section 5 presents the model fits, Section 6 discusses the model implications, and Section 7 draws conclusions.

2 CENTAURUS A

Centaurus A, the famous southern FR I (Fanaroff & Riley 1974) radio counterpart to NGC 5128, identified by Bolton, Stanley & Slee (1949), lies at a distance of approximately 3.1 Mpc (1 arcsec = 15 pc, at this distance) (Tonry & Schechter 1990), and is a multifaceted object. It shows evidence of a merger, star formation and AGN activity, with H II regions, shells, jets, optical filaments, an X-ray halo and a warped dust lane [see Israel (1998) for a comprehensive review]. It is perhaps most notable at optical wavelengths for the dramatic dust lane [at a position angle (PA) of $\sim 110°$ and $\sim$ 5-kpc extent] that bisects the host galaxy NGC 5128 and is recognized as being an 'active' region of star formation with dust, gas and H II regions (e.g. Graham 1979).

Marston & Dickens (1988) found that their 12-μm *IRAS* DSD observations followed the warping in the dust lane and the extensions to the south-east and north-west, coincident with the 10-μm imaging of Telesco (1978), 60-μm imaging and Hα emission, and hence the regions of star formation. They modelled their 12-, 25-, 60- and 100-μm observations as a cirrus spectrum of small and large grains heated by the interstellar radiation field. Two grain temperatures were invoked [hot (240 K) small grains and cooler (30 K) large grains]; the ratio of hot to cool dust was highest around the nuclear region and dropped off as more galaxy was included. They determined a star formation rate of $9.8\,M_{\odot}\,yr^{-1}$, comparable to that of the starburst galaxy M83. Similarly, Eckart et al. (1990), using $L_{FIR}/M(H_2)$ as a measure of star formation, obtained a figure of $24\,L_{\odot}/M_{\odot}$, consistent with values for galaxies exhibiting starburst activities, whilst Adams, Adamson & Giles (1983), using observations of young blue stars, found the disc of Centaurus A to be similar to that of M82.

Recent MIR ISOCAM and submillimetre SCUBA imaging (Mirabel et al. 1999) has dramatically shown a highly inclined barred spiral galaxy within the host galaxy NGC 5128, providing strong evidence for both considerable dust emission from star formation and the merger hypothesis for the morphology of Centaurus A. Interestingly, on small size-scales ($r \sim 200$ pc) a structure is observed with a PA of 145°, perpendicular to the axis of the radio jets and at the same PA as the NIR nuclear polarization (Packham et al. 1996), suggesting an association with the AGN. This structure has been observed before [e.g. in the submillimetre (Hawarden et al. 1993), IR (Joy et al. 1988; Eckart et al. 1990), CO (Eckart et al. 1990; Israel et al. 1990, 1991; Rydbeck et al. 1993)], although not in such striking detail.

Centaurus A has considerable evidence of AGN activity, although the nucleus remains obscured with no evidence for broad lines in either total flux (Simpson & Meadows 1999) or polarized flux (Alexander et al. 1999). The direct visual extinction to the nucleus is high, measured by Blanco, Ward & Wright (1990) as ~ 70 mag from X-ray observations, and by Turner et al. (1992) as between 38 and 55 mag, by re-evaluating the depth of the 9.7-μm silicate feature of Grasdalen & Joyce (1976). NIR imaging polarimetry (Packham et al. 1996) has shown an enhancement of polarization around the nucleus, interpreted as scattered radiation from the central source, although there could also be a significant component of dichroic absorption (Alexander et al. 1999). Although Centaurus A is the nearest discovered radio-loud AGN, emission at MIR wavelengths from the central source is unresolved, putting constraints on the size of the 10-μm emission region of < 1 arcsec (Israel 1998).

All of the above evidence can be interpreted as a heavily obscured central continuum region (for example, an accretion disc surrounded by an optically and geometrically thick torus) which is then itself surrounded by a larger circumnuclear region related to the AGN – all at a PA of $\sim 145°$. On larger kiloparsec scales the dust lane dominates at a PA of $\sim 110°$, where large-scale star formation has been occurring.

3 OBSERVATIONS AND DATA

The observations used to constrain the models have been taken from a variety of sources and are grouped into three aperture sizes: a small, nuclear aperture of ~ 4 arcsec; an intermediate aperture of ~ 20 arcsec; and a large aperture of ~ 90 arcsec. The data sources and information are presented in Table 1 and Fig. 1.

In the NIR, care has to be taken to correct for the contribution from starlight, and we have only chosen small-aperture data from the literature where such corrections have been applied. Hawarden et al. (1993) found an aperture dependence in the submillimetre to millimetre spectrum of Centaurus A. In the small nuclear aperture (FWHM < 6 arcsec) a non-thermal variable source dominates. This source was found to have an essentially flat spectrum, and the submillimetre to millimetre data have had this contribution

Table 1. Observations.

Wavelength (μm)	Beamsize	Telescope/instrument	Reference
(a) Nuclear aperture			
2.2 and 3.3	2.5 arcsec	IRTF/Rochester NIR array camera	(a), (b)
7.8–13.0	4.3 arcsec	AAT/UCL spectrometer	(c)
(b) Intermediate aperture			
6.0–13.0	24×24 arcsec^2	ISOPHOT_S	(c)
6.9–10.5	14×20 arcsec^2	ISOSWS	(c), (d)
12.3–26.0	14×27 arcsec^2	ISOSWS	(c), (d)
28.3	20×27 arcsec^2	ISOSWS	(c), (d)
34.9	20×33 arcsec^2	ISOSWS	(c), (d)
350, 450 and 1100	18 arcsec	JCMT/UKT14	(e)
800 and 850	17 arcsec	JCMT/UKT14	(e)
1300	20 arcsec	JCMT/UKT14	(e)
(c) Large aperture			
12, 25, 60 and 100	~ 90 arcsec	*IRAS*/broad-band photometer	(f)
370, 770 and 1070	80 arcsec	UKIRT/QMC photometer	(g)

References: (a) Packham et al. (1996); (b) Turner et al. (1992); (c) this paper; (d) Sturm et al. (in preparation); (e) Hawarden et al. (1993); (f) data taken from the NED (from the *IRAS* Faint Source Catalog: Moshir et al. 1990); (g) Cunningham et al. (1984).

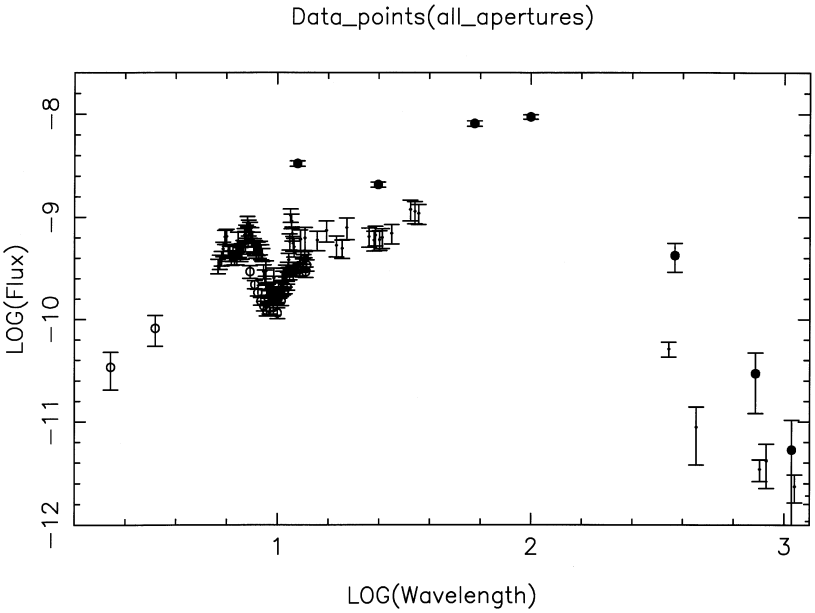

Figure 1. The data applied to the model. The nuclear-aperture data points are shown as open circles (see Table 1a), the intermediate-aperture points are shown as small points (see Table 1b) and the large-aperture points are shown as filled circles (see Table 1c). The wavelength units are log(μm); the flux units are νF_ν [log(erg s^{-1} cm^{-2})].

removed; the effect that this has on the FIR observations is negligible (Joy et al. 1988).

3.1 UCL spectrometer observations

The UCL spectrometer (Aitken & Roche 1982) observations were taken in 1984 May at the 3.9-m Anglo-Australian Telescope in a nuclear, 4.3 arcsec, aperture (see Table 1a), and are shown in Fig. 2. The total exposure time was 2400 s. The shape, features and fluxes are very similar to those in the higher signal-to-noise ratio ISOCAM CVF spectrum of Mirabel et al. (1999), which was obtained in a similar sized aperture. We have measured the depth of the Si feature as $\tau_{9.7} = 1.0$, using a simple linear continuum fit and measuring the depth of absorption at the 9.7-μm point. The presence of hot dust will fill in the feature, so this extinction should be taken as a lower limit. The conversion from $\tau_{9.7}$ to A_v is dependent on metallicity (Roche & Aitken 1985), making an accurate estimation of the visual extinction uncertain; however, assuming the interstellar medium metallicity gives $A_v = 19$ mag. The feature at 12.8 μm is [Ne II] (see Roche et al. 1991), and the feature between 11.2 and 11.8 μm is probably 11.3-μm PAH (see Section 5.1) as seen in the ISOPHOT_S spectrum and the higher signal-to-noise ratio spectrum of Mirabel et al. (1999).

3.2 ISOPHOT_S and ISOSWS observations

The ISOPHOT_S and ISOSWS observations were taken with the *Infrared Space Observatory* (*ISO*: Kessler et al. 1996).

The ISOPHOT_S (Lemke et al. 1996) observations were taken in 1996 February in an intermediate, 24 arcsec, aperture (see Table 1b), and are shown in Fig. 3. The total exposure time was 1130 s. The observations have been reduced with PIA without

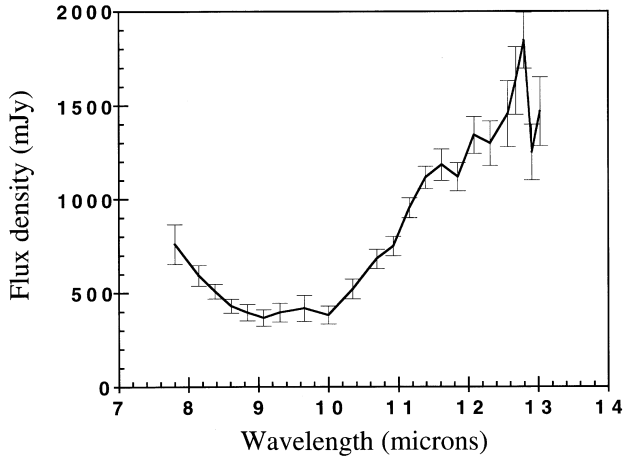

Figure 2. The UCL spectrometer observations.

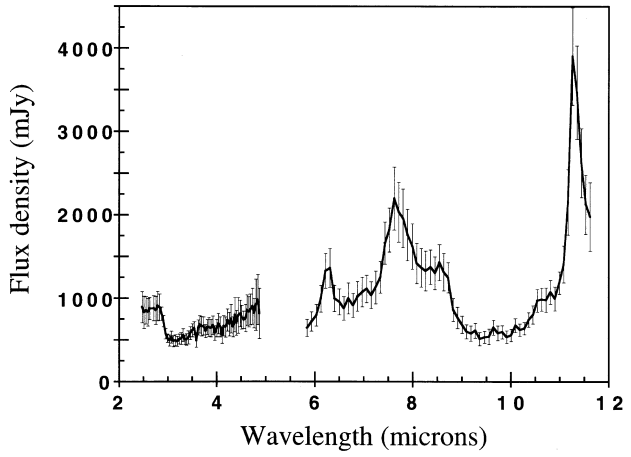

Figure 3. The ISOPHOT_S observations.

additional modifications. The zodiacal light contributions have been removed using a chopped measurement. The ISOPHOT_S spectrum consists of two parts: PHT_SL (6–12 μm) and PHT_SS (2.5–5.5 μm). Clearly seen in the spectrum are the deep 9.7-μm Si feature and 6.3-, 7.7-, 8.6- and 11.3-μm PAH features; however, importantly, PAH emission at 3.3 μm is not clearly detected. The depth of the Si feature is difficult to determine, owing to the presence of PAH features. Applying a linear continuum fit that retains the PAH features gives $\tau_{9.7} = 1.0$, the same as that determined with the UCL spectrometer observations.

As our radiative transfer codes do not take account of atomic and molecular line emission, the ISOSWS (de Graauw et al. 1996) observations presented here are the line-free continuum points. The emission-line spectrum, details of the observations and data reduction are presented in Sturm et al. (in preparation). The continuum points were determined by a second-order polynomial fit to the line-free regions of the data (the continuum either side of the emission line). The error bars represent the uncertainty in flux calibration – the rms noise level is insignificant by comparison. These observations come from a range of intermediate aperture sizes (see Table 1b). No correction has been made for the different wavelength aperture sizes.

Owing to the problem of starlight contribution, and some uncertainty in the flux levels at the short-wavelength end of these spectra, the data shortward of 6 μm are not used in the model fitting.

4 THE INFRARED MODEL

The proposed model for Centaurus A is the combination of a number of components, as outlined below.

4.1 Torus

The torus model is essentially that discussed in detail by EHY. The method of obtaining the intensity distribution at any point in the torus, and hence iterating for the temperature, is that used by Efstathiou & Rowan-Robinson (1990) and ER95.

In trying to fit to the global IR properties of AGN, the best toroidal shape was found by ER95 to be a tapered disc. Flared discs and anisotropic spheres do not give the correct properties – in particular the 9.7-μm Si feature, seen in absorption in type 2 AGN but not in emission in type 1 AGN, is difficult to model, as is the width of the spectral energy distribution (SED). Essentially the torus emission is a superposition of emission from dust at different temperatures, in the range 1000–100 K, showing differing intensities of NIR, MIR and FIR emission, depending on the regions observed. An edge-on torus would show more cool than hot dust (more FIR than NIR emission), whilst a face-on torus would show the hottest regions of dust as well as cooler dust (approximately equal NIR and FIR emission).

The main model parameters are the opening half-angle of the toroidal cone (Θ), the ratio of the inner and outer radii (r_1/r_2), the ratio of the height to the outer radius (h/r_2), the equatorial optical depth ($^{e}\tau_{uv}$), the dust sublimation temperature (T_1) and the radial dependence of the density distribution ($r^{-\beta}$).

The EHY model of NGC 1068 also assumed a component of optically thin hot dust, located in the cone of the torus. This gave, for NGC 1068, a better fit to the NIR emission (simply tilting the torus to give more NIR gave a poorer fit to the 9.7-μm Si feature). Such a component of hot dust is consistent with the 3–5 μm bump in AGN (corresponding to ~1000-K hot dust), the additional extinction to the broad-line region observed in type 1 AGN (Ward et al. 1987) and the differential extinction between the NIR and X-ray emission regions (e.g. Alonso-Herrero, Ward & Kotilainen 1997). The hot dust was modelled as a density distribution of r^{-2}.

4.2 Starburst

The starburst component is described in detail by ERS. The emission of the transiently heated particles is calculated according to the method of Siebenmorgen & Krügel (1992). Proper treatment of the photodestruction of the PAHs and the sublimation of the large grains, at the inner edge of the cloud, is taken into account. The grain model used is that of Siebenmorgen & Krügel (1992), where the grains are assumed to have a power-law size distribution [$n(a) \propto a^{-q}$, $q = 3.5$, $5 \leq a \leq 2500$ Å]. Three populations of dust particles are treated:

(i) Mathis, Rumpl and Nordsieck type large particles with the optical constants for 'astronomical' silicates taken from Draine & Lee (1984) and the amorphous carbon taken from Edoh (1983);

(ii) small graphite grains to account for the extinction bump around 2175 Å (Draine 1989);

(iii) PAH molecules and clusters to explain the NIR and MIR emission bands (Allamandola, Tielens & Barker 1989; Puget & Leger 1989).

The starburst model assumes that the starburst is made up of an

ensemble of giant molecular clouds centrally illuminated by hot stars. The stellar population is modelled in terms of the population synthesis models of Bruzual & Charlot (1993), and the giant molecular clouds are assumed to evolve with time owing to the expansion of the H II regions. The model has been successfully applied to the SEDs of M82 and NGC 6090.

4.3 Cirrus

The cirrus contribution is computed using the same grain model as for the starburst, although in this case adopting the PAH parameters used by Siebenmorgen & Krügel (1992) to fit the emission from the local neighbourhood. As the cirrus emission is widely assumed to be due to diffuse dust, there is no need to perform a radiative transfer calculation. However, for the sake of convenience we have used the spherically symmetric code of ERS to model the cirrus as a centrally illuminated optically and geometrically thin dust shell.

The central source in this case is assumed to be a 12 000-K blackbody, and the temperature of the large grains at the inner edge of the shell is assumed to be 40 K. The resultant spectrum gave a very good fit to observations of cirrus towards the centre of the Galaxy (Rowan-Robinson 1992). This model is similar to that proposed by Siebenmorgen & Krügel (1992).

4.4 Dust lane

To take account of dust lane absorption, radiation from the torus and starburst are visually extinguished by 10 mag, essentially the same as the value adopted by Packham et al. (1996). The cirrus is not extinguished since it is itself associated with the dust lane. The extinction model used assumes the grain model and interstellar extinction curve of Rowan-Robinson (1992).

5 MODEL FITS

For small apertures, and at IR wavelengths below 12 μm we initially assumed the SED to be dominated by radiation from the torus, seen through the dust lane. We therefore fitted the torus model to this wavelength range, which includes the 9.7-μm Si feature. In fitting to the larger apertures we have included the contribution from the smaller apertures and added any additional components required.

5.1 Nuclear aperture

Without strong observational evidence to the contrary, we have assumed that the Centaurus A torus is similar to that of NGC 1068, an assumption made with strong observational and modelling evidence (e.g. EHY; Young et al. 1996; Granato, Danese & Franceschini 1997). We set all the torus parameters, except for the inclination, to the same values as in the EHY model for NGC 1068 [$\Theta = 30°$ (see Section 6); $r_1/r_2 = 0.01$; $h/r_2 = 0.1$; ${}^{e}\tau_{uv} = 1200$; $T_1 = 950$ K; and $\beta = -1$: see Section 4.1], and then calculated the SED for various values of inclination (i, the angle between the polar axis and the line of sight). Fig. 4 shows a selection of SEDs for $i = 40°$, 70° and 90°. No value of inclination gave a simultaneously good fit to both the NIR continuum and the Si feature, with the former best fitted by $i = 40°$ and the latter by $i = 70°$.

The observed Si feature shows an additional feature between 11.2 and 11.8 μm, which cannot be fitted by the torus model and which we believe is emission from 11.3-μm PAH (as seen in the spectrum of Mirabel et al. 1999). We therefore added a component of starburst (see Section 4.2). This provided an excellent fit to the Si feature, with roughly equal components of torus and starburst for wavelengths less than 60 μm, with the torus at an inclination of 45° (see Fig. 5). The feature at 12.8 μm is [Ne II] which has not been modelled.

For larger apertures (see Sections 5.2 and 5.3) a component of cirrus emission is required (see Section 4.3). For completeness, the contribution that this would make in the nuclear aperture is shown in Fig. 5 (the cirrus component was determined by assuming constant surface brightness, as implied from the fits in

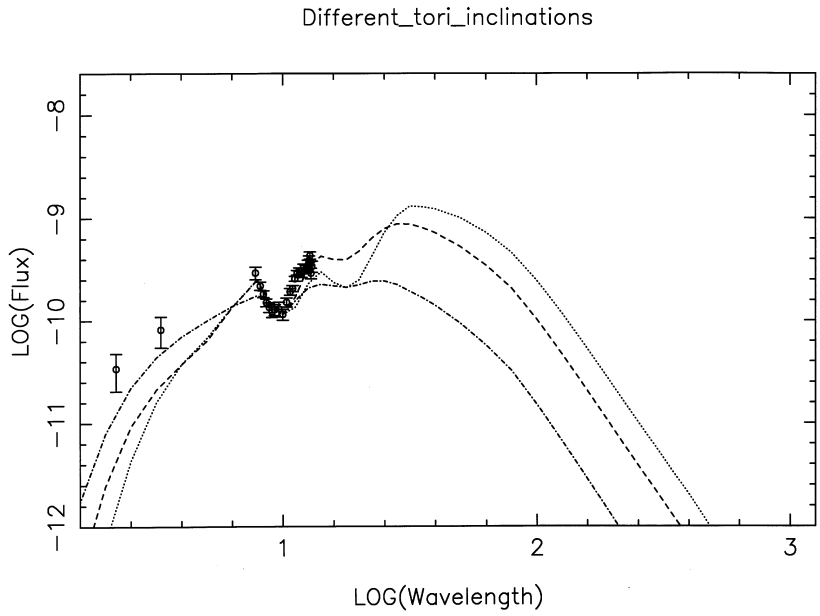

Figure 4. The torus model, fitted to the nuclear-aperture points, for a range of inclinations: 40° (dot–dashed line); 70° (dashed line); 90° (dotted line). The axial units are the same as in Fig. 1.

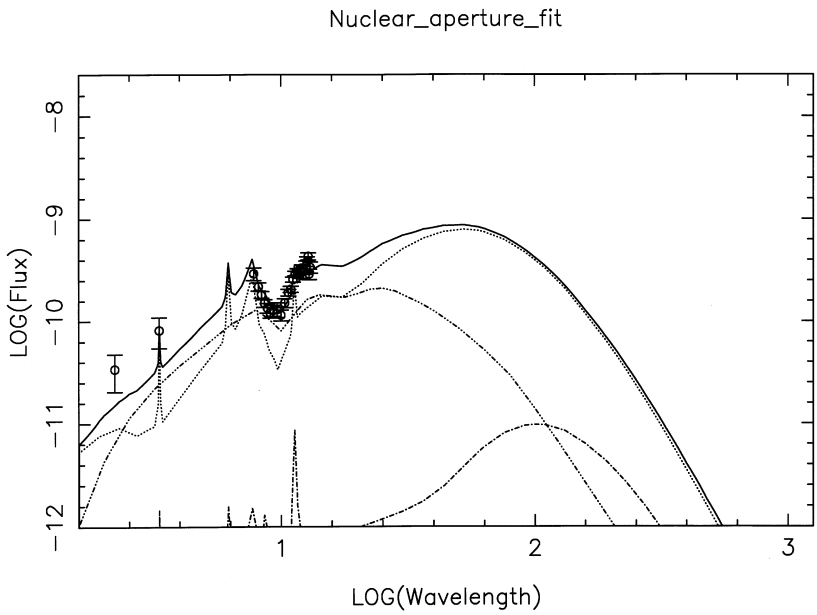

Figure 5. The model fit to the nuclear-aperture points. The torus spectrum is shown as a dash–triple-dotted line; the starburst spectrum is shown as a dotted line; and the cirrus spectrum is shown as a dot–dashed line. The combination of the components is shown as a thick line. The axial units are the same as in Fig. 1.

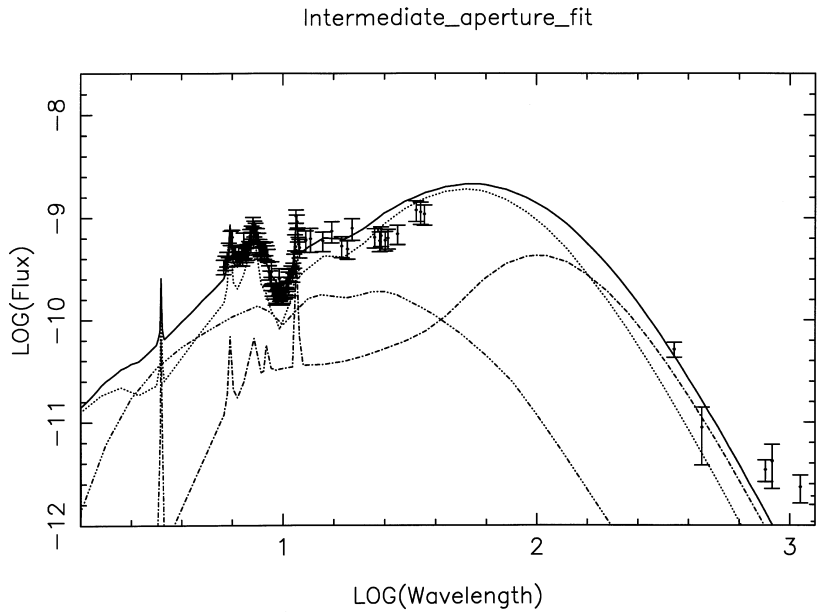

Figure 6. The model fit to the intermediate-aperture points; see Fig. 5 for line key. The axial units are the same as in Fig. 1.

the larger apertures: see Fig. 8, later). As can be seen, the cirrus contribution is negligible for the nuclear aperture.

5.2 Intermediate aperture

Here we kept the torus component fixed (i.e. we assumed that there is no contribution beyond 4 arcsec; see Section 6 for analysis and comment) and added an additional contribution from the starburst, producing a reasonable fit to the intermediate-aperture data points for the Si feature, and the IR continuum below 25 μm. The PAH features between 7 and 12 μm and the continuum at longer wavelengths showed that an additional component was required. Observations (e.g. Marston & Dickens 1988; Telesco 1978) suggest that this additional component is cirrus emission within the dust lane. By slightly reducing the contribution from the starburst and adding a component of cirrus, an excellent fit to the Si and 6–12 μm PAH features, and a better fit to the IR and submillimetre continuum was obtained (see Fig. 6). A better fit to the submillimetre points could be made by substituting the 40-K cool cirrus dust component with that of a 30-K dust component, consistent with the figure suggested by Marston & Dickens (1988) for the large-grain population of cirrus, but inconsistent with the generic cirrus model presented by ERS. The starburst component is well constrained by the Si feature, and the cirrus component is well constrained by the PAH features.

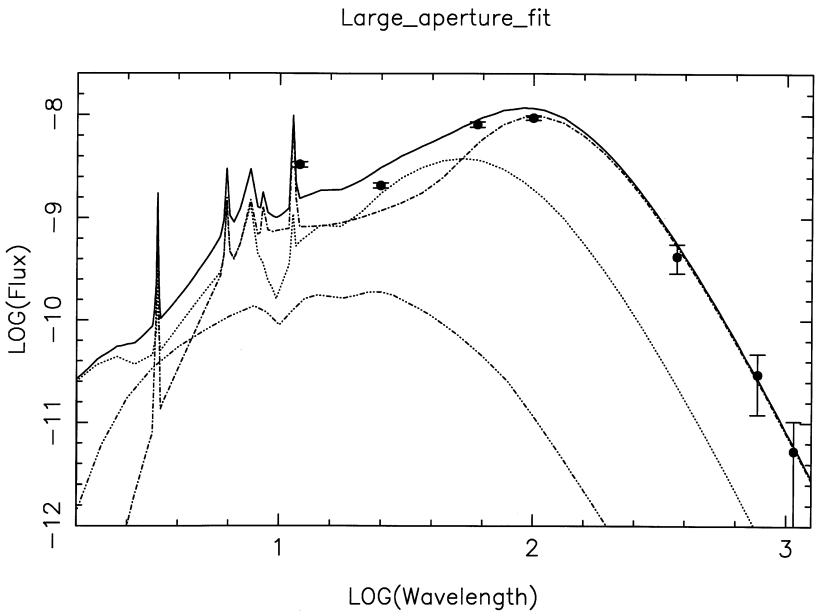

Figure 7. The model fit to the large-aperture points; see Fig. 5 for line key. The axial units are the same as in Fig. 1.

5.3 Large aperture

The best fit to the large aperture is obtained with a relatively small increase (a factor of 2) in the starburst contribution and a significant increase in the cirrus contribution (a factor of 23) (see Fig. 7). Although the 12-μm data point does not fit very well, the *IRAS* filter is broad at 12 μm and a contribution from 11.3-μm PAH would be included within this data point. This moderate increase in the starburst contribution over a large increase in aperture size suggests that the most vigorous star formation is occurring close to the nucleus.

6 DISCUSSION

The complete model includes contributions from torus, starburst and cirrus in all apertures, and is shown graphically in Fig. 8. The computed model torus characteristics are presented in Table 2.

Observational support for the size of our model torus comes from 2.3-GHz radio observations of the nuclear subarcsec-scale jet and counter-jet (Jones et al. 1996). These images show the core to be completely absorbed between the jet and counter-jet; this absorption is attributed to that produced by a gaseous disc or torus of 0.4–0.8 pc radius. Our model torus, with a height and radius of 0.18 and 1.8 pc, respectively, at an inclination of 45°, would present a 1.4-pc absorption band, very similar to the size of the radio core absorption. The calculated torus diameter of 3.6 pc places it easily within the nuclear aperture (∼ 4 arcsec, 60 pc), and is consistent with the observations of an unresolved (< 1 arcsec, < 15 pc) 10-μm source (Israel 1998). The torus inner radius (0.018 pc, ∼ 3700 au) would project an angular size of ∼ 1 milliarcsec and would most likely be the location of any H_2O maser emission; however, as this emission has not been detected in Centaurus A (Braatz, Wilson & Henkel 1996), perhaps because of the low power of the torus or beaming of the megamaser emission away from the line of sight, this parameter cannot be verified. Based on this inner dust sublimation radius, the luminosity of the enclosed central source can be estimated from Granato, Danese & Franceschini. (1997) and is of the order of $10^{43}\,\mathrm{erg\,s^{-1}}$, in good agreement with Israel (1998). Observational support for the opening half-angle of the toroidal cone ($\Theta = 30°$) comes from high-resolution NIR imaging (Bryant & Hunstead 1999), which shows a nuclear cone structure of $\Theta = 30° \pm 5°$, and the recently published *Hubble Space Telescope* nuclear Paα image (Schreier et al. 1998). This latter image shows a cone-like structure of ∼ 30° opening half-angle and ∼ 3-arcsec extent at the same location, and of the same extent, as the polarized structure seen in the lower resolution *K*-band imaging polarimetry of Packham et al. (1996), implying that this structure may be an ionization cone rather than the suggested warped accretion disc. The extinction to the 2.2-μm region can be estimated by comparing the flux of the face-on torus with that of the 45° inclined torus and is 2.6 mag, equating to a visual extinction of ∼ 30 mag. This degree of extinction is consistent with the analysis of Giles (1986) and Meadows & Allen (1992), and is consistent with the NIR emission region being considerably less extinguished than the X-ray region (see Sections 2 and 4.1).

The calculated torus diameter of 3.6 pc is significantly smaller than that observed in other galaxies [e.g. ∼ 1 kpc for MG 0414 + 0534 (Oya et al. 1999), ∼ 200 pc for NGC 1068 (Young et al. 1996), ∼ 100 pc for NGC 4261 (Jaffe et al. 1993) and ∼ 50 pc for NGC 4151 (Mundel et al. 1995)]. Centaurus A is a low-luminosity AGN, as is evident from its hard X-ray continuum (Morini, Anselmo & Molteni 1989) and FR I classification (Fanaroff & Riley 1974), and, although there is no good evidence, the small torus size that we estimate for Centaurus A may well indicate a connection between the size of the torus and the central source luminosity. Although of a small diameter, this torus model does not support the even smaller diameter tori of Pier & Krolik (1992) which, by comparison, would suggest a torus diameter of ⩽ 1 pc. In contrast, the Granato et al. (1997) axially symmetric flared disc model would predict a torus of similar size to that presented here.

Recent geometrical modelling of high-resolution NIR imaging has suggested that the torus in Centaurus A has a diameter of 240 ± 20 pc (Bryant & Hunstead 1999) and an inner radius of 40 pc at a PA of ∼ 145° – consistent with the structure observed in CO by Israel et al. (1990). However, as highlighted by Israel

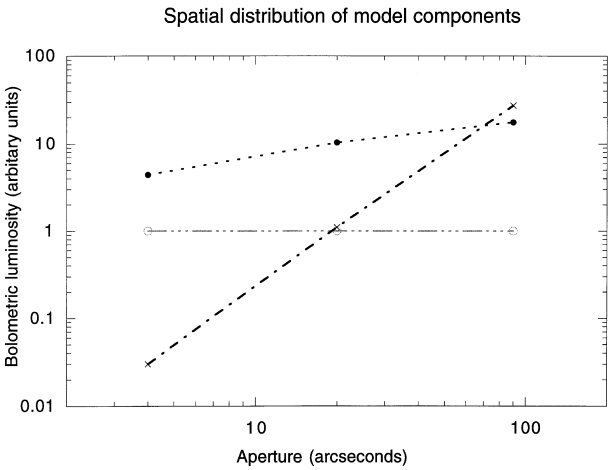

Figure 8. The spatial distribution of the model components. The torus (dash–triple-dotted line) is unchanged; the cirrus (dot–dashed line) follows constant surface brightness; the starburst (dotted line) is most dominant in the small apertures.

Table 2. Model torus characteristics.

Parameter	Description	Value
i	Polar inclination from line of sight	45°
r_1	Torus inner radius	0.018 pc (~ 3700 au)
r_2	Torus outer radius	1.8 pc
h	Torus height	0.18 pc
s	Torus size as projected on sky	$3.6 \times 2.7\,\mathrm{pc}^2$
Θ	Torus cone opening half-angle	30°

Note: dimensions are calculated assuming a distance of 3.1 Mpc.

(1998), this structure most likely represents a larger circumnuclear region and not the dusty AGN torus itself, as it is too distant to feed the AGN and collimate the nuclear jet/cone structure. Additionally, if this structure represented the dusty AGN torus then the inner radius would most reasonably be defined as the dust sublimation point, suggesting an improbably high central source luminosity (of order $5 \times 10^{49}\,\mathrm{erg\,s^{-1}}$), in conflict with other observations. Within our model we interpret this structure as an inner starburst region which appears to be associated in some way with the AGN and inner dusty torus. The dusty AGN torus model that we present here would be responsible for feeding the AGN and collimating the nuclear jet/cone structure.

Within the context of unified theories, the inclination of the torus is a crucial parameter in determining whether an AGN is of type 1 or type 2. Various studies have suggested that the *IRAS* 60/25-μm flux density ratio is an indicator of torus inclination, with high and low ratios implying edge-on and face-on torus inclination respectively. Fig. 7 shows the effect of the inclusion of *IRAS* points on the Centaurus A model. The combination of all the model components gives a 60/25-μm flux density ratio of 9.4, although the actual torus 60/25-μm flux density ratio is only 0.7. If the torus were as powerful as that in NGC 1068, or a smaller nuclear-sized aperture were used, the 60/25-μm flux density ratio would be more indicative of the torus inclination angle, but, within the large *IRAS*-sized aperture, the torus is dominated by other more powerful IR-emitting components. Striking evidence of this comes from the ISOLWS FIR continuum of the archetypal Seyfert 2 galaxy (NGC 1068), in which the FIR continuum is almost indistinguishable from that of the archetypal starburst galaxy (M82) (Spinoglio et al. 1999).

7 CONCLUSIONS

We have presented new ISOSWS, ISOPHOT_S and 8–13 μm observations of Centaurus A. We have applied radiative transfer models to these observations to develop a model for the infrared continuum. We find that, in a small nuclear aperture (~ 4 arcsec, ~ 60 pc), the SED is characteristic of components of both starburst and torus. In larger apertures, additional components of cirrus and starburst are required. Our modelling is supported by observations from NIR to millimetre wavelengths. Based on our model, the torus diameter and height are 3.6 and 0.18 pc, respectively, and the torus is inclined at an angle of 45°. We have presented independent observational evidence for such a structure. This small size has implications for the detectability of tori in other low-power AGN, and for the use of the *IRAS* 60/25-μm flux density ratio as an indicator of torus inclination. In the large *IRAS* apertures the 60/25-μm flux density ratio is found to be 9.4, whilst the torus itself has a 60/25-μm flux density ratio of only 0.7. The ratio is dominated by the cirrus and starburst components that are powerful in the FIR.

ACKNOWLEDGMENTS

We thank the referee, Alberto Franceschini, for useful comments which have improved the balance of this paper. DMA acknowledges PPARC for studentship support during this work, and is currently in receipt of an EC TMR network (FMRX-CT96–0068) postdoctoral grant. AE acknowledges PPARC for postdoctoral support. This research has made use of the NASA/IPAC Extragalactic Database (NED), which is operated by the Jet Propulsion Laboratory, California Institute of Technology, under contract with NASA.

REFERENCES

Adams D. J., Adamson A. J., Giles A. B., 1983, MNRAS, 202, 241
Aitken D. K., Roche P. F., 1982, MNRAS, 200, 217
Alexander D. M., Hough J. H., Young S., Bailey J. A., Heisler C. A., Lumsden S. L., Robinson A., 1999, MNRAS, 303, L17
Allamandola L. J., Tielens A. G. G. M., Barker J. R., 1989, ApJS, 71, 733
Alonso-Herrero A., Ward M. J., Kotilainen J. K., 1997, MNRAS, 288, 977
Antonucci R., 1993, ARA&A, 31, 473
Blanco P. R., Ward M. J., Wright G. S., 1990, MNRAS, 242, 4p
Bolton J. G., Stanley G. J., Slee O. B., 1949, Nat, 164, 101
Braatz J. A., Wilson A. S., Henkel C., 1996, ApJS, 106, 51
Bruzual G., Charlot S., 1993, ApJ, 405, 538
Bryant J. J., Hunstead R. W., 1999, MNRAS, submitted, (astro-ph/9811481)
Cunningham C. T., Ade P. A. R., Robson E. I., Radostitz J. V., 1984, MNRAS, 211, 543
Draine B. T., 1989, in Allamandola L., Tielens A. G. G. M., eds, Proc. IAU Symp. 135, Interstellar Dust. Kluwer, Dordrecht, p. 313
Draine B. T., Lee H. M., 1984, ApJ, 285, 89
Eckart A., Cameron H., Rothermel H., Wild W., Zinnecker H., Rydbeck G., Olberg M., Wiklind T., 1990, ApJ, 363, 451
Edoh O., 1983, PhD thesis, University of Arizona
Efstathiou A., Hough J. H., Young S., 1995, MNRAS, 277, 1134(EHY)
Efstathiou A., Rowan-Robinson M., 1990, MNRAS, 245, 275
Efstathiou A., Rowan-Robinson M., 1995, MNRAS, 273, 649(ER95)

Efstathiou A., Rowan-Robinson M., Siebenmorgen R., 1999, MNRAS, in press (ERS)
Fanaroff B. L., Riley J. M., 1974, MNRAS, 167, 31p
Giles A. B., 1986, MNRAS, 218, 615
de Graauw T. et al., 1996, A&A, 315, L49
Graham J. A., 1979, ApJ, 232, 60
Granato G. L., Danese L., Franceschini A., 1997, ApJ, 486, 147
Grasdalen, G. L., Joyce R. R., 1976, ApJ, 208, 317
Hawarden T. G., Sandell G., Matthews H. E., Friberg P., Watt G. D., Smith P. A., 1993, MNRAS, 260, 844
Israel F. P., 1998, A&AR, 8, 237
Israel F. P., van Dishoeck E. F., Baas F., de Graauw T., Phillips T. G., 1991, A&A, 245, L13
Israel F. P., van Dishoeck E. F., Baas F., Koornneef J., Black J. H., de Graauw T., 1990, A&A, 227, 342
Jaffe W., Ford H. C., Ferrarese L., van den Bosch F., Connell R. W., 1993, Nat, 364, 213
Jones D. L. et al., 1996, ApJ, 466, L63
Joy M., Lester D. F., Harvey P. M., Ellis H. B., 1988, ApJ, 326, 662
Kessler M. F. et al., 1996, A&A, 315, L27
Krügel E., Siebenmorgen R., 1994, A&A, 282, 467
Lemke D. et al., 1996, A&A, 315, L64
Marston A. P., Dickens R. J., 1988, A&A, 193, 27
Meadows V., Allen D., 1992, Proc. Astron. Soc. Aust., 10(2), 104
Mirabel I. F. et al., 1999, A&A, 341, 667
Morini M., Anselmo F., Molteni D., 1989, ApJ, 347, 750
Moshir M. et al., 1990, IRAS Catalogs, The Faint Source Catalog, version 2.0. JPL, Pasadena
Mundel C. G., Pedlar A., Baum S. A., O'dea C. P., Gallimore J. F., Brinks E., 1995, MNRAS, 272, 355
Oya S., Iwamuru F., Iwai J., Tsukamoto H., Maihora T., 1999, in Cox P., Demuyt V., Kessler M., eds, Proc. ESO Symp., The Universe as Seen by ISO. ESA Special Publications Series (SP-427), Paris, in press
Packham C., Hough J. H., Young S., Chrysostomou A., Bailey J. A., Axon D. J., Ward M. J., 1996, MNRAS, 278, 406
Pier E., Krolik J., 1992, ApJ, 401, 99
Puget J. L., Leger A., 1989, ARA&A, 27, 161
Roche P. F., Aitken D. K., 1985, MNRAS, 215, 425
Roche P. F., Aitken D. K., Smith C. H., Ward M. J., 1991, MNRAS, 248, 606
Rowan-Robinson M., 1992, MNRAS, 258, 787
Rowan-Robinson M., Crawford J., 1989, MNRAS, 238, 523
Rowan-Robinson M., Efstathiou A., 1993, MNRAS, 263, 675
Rydbeck G., Wiklind T., Cameron M., Wild W., Eckart A., Genzel R., Rothermal H., 1993, A&A, 270, L13
Schreier E. J. et al., 1998, ApJ, 499, L143
Siebenmorgen R., Krügel E., 1992, A&A, 259, 614
Simpson C., Meadows V., 1999, ApJ, submitted (astro-ph/9807313)
Spinoglio L. et al., 1999, in Cox P., Demuyt V., Kessler M., eds, Proc. ESO Symp., The Universe as Seen by ISO. ESA Special Publications Series (SP-427), Paris, in press
Stark R., 1995, A&A, 301, 873
Telesco C. M., 1978, ApJ, 226, L125
Tonry J. L., Schechter P. L., 1990, AJ, 100, 1794
Turner P. C., Forrest W. J., Pipher J. L., Shure M. A., 1992, ApJ, 393, 648
Ward M. J., Geballe T., Smith M., Wade R., Williams P., 1987, ApJ, 316, 138
Young S., Packham C., Hough J. H., Efstathiou A., 1996, MNRAS, 283, L1